DOI 10.1007/s12541-009-0069-1

Advanced Parameter Identification for a Linear-Motor-Driven Motion System Using Disturbance Observer

Yi-Ren Pan[1], Yi-Ti Shih[2], Rong-Hwang Horng[1] and An-Chen Lee[1,#]

1 Department of Mechanical Engineering, National Chiao-Tung University, Hsinchu, Taiwan, ROC, 30010
2 ICP DAS CO., LTD, No. 111, Guangfu N. Rd., Hukou Township, Hsinfhu County, Taiwan, ROC, 30351
Corresponding Author / E-mail: aclee@mail.nctu.edu.tw, TEL: +886-3-5712121, FAX: +886-3-5725372

KEYWORDS: Disturbance observer, Linear-motor-driven motion system, System identification

Disturbance observer (DOB) is generally introduced into motion control systems to eliminate undesired disturbances and plant uncertainty. The DOB is also used for system identification. This work presents a novel experimental identification algorithm using disturbance observer to identify inertia, viscous coefficient, and friction of linear-motor-driven motion system. A conventionally adopted algorithm for determining the inertia of the motion system based on orthogonal relations among system responses is modified and extended to estimate the viscous coefficient and the magnitude of Coulomb friction of the underlying system. The advantages of the proposed method are high convergence rate and only one experiment needed to evaluate the system parameters. The proposed algorithm is demonstrated to be workable by both simulation and experiment.

Manuscript received: August 21, 2008 / Accepted: June 1, 2009

1. Introduction

Linear slide systems are one of the most common applications of motion control. Most linear slide systems are ball-screw-driven, but linear-motor-driven systems become popular in recent years because of their simple structures and an absence of flexible coupling. Backlash and compliance in a ball-screw-driven system may induce nonlinear phenomena and multi-source friction effects,[1] preventing the distinguishing of friction from other nonlinear effects. By contrast, linear-motor-driven systems are free from such complexities because of the nonexistence of a nonlinear backlash and multi-source friction. The observed friction behaviors of the two systems differ for the same reason.

In servo motor drive applications, variation of inertia, viscous coefficient, and friction degrades drive performance. Once the principle parameters of motors are found, the motion control loop gains can be tuned automatically in order to maintain a consistent dynamic response.[2] Owing to the nonlinear characteristics of velocity-dependent friction term, the three parameters (inertia, viscous coefficient, and friction) can be hardly estimated simultaneously using classical identification method easily, e.g., the least square method.[3] The common approach would be the separate identification of the friction parameter. In this approach, at first the friction parameter using constant velocity motion is identified. This parameter is then considered to be known for the identification of the other parameters.[4,5] Analogously, one can perform a lot of time-consuming experiments to build up the friction-velocity map, then to identify the viscous coefficient, and friction parameters from the map.[6] However, these simple methods induce the risk of error accumulation between two steps. Other methods have also been proposed to estimate the moment of inertia, for example, recursive extended least square, Kalman filter, and Lunberger-type state observer.[7-9] Kim[10] presented a sequential parameter auto-tuning algorithm at motion startup. The flux linkage and the disturbance torque were estimated separately from two reduced-order observers. Then, the inertia was obtained from the orthogonal property of the periodic speed reference; however, the controlled bandwidth might decrease due to the lack of viscous coefficient identification.

In recent years, the disturbance observer (DOB) has been introduced into motion control systems to eliminate as much of the "equivalent disturbance" as possible, and to force the actual system to become a nominal model. The equivalent disturbance consists of

external disturbance signals which include friction and signals associated with model uncertainties and nonlinearity. If these uncertainties are eliminated by disturbance observer, the linear feedback controller can be applied to construct an asymptotically stable system. Ohnishi[11] introduced this equivalent disturbance, which was refined by Umeno and Hori.[12] Lee and Tomizuka[13] and other researchers[14-26] demonstrated the effectiveness of the disturbance observer by performing experiments with various uncertainties and external disturbances, to improve performance in tracking or point-to-point control.

The disturbance observer (DOB) is also used for parameter identification. Kobayashi *et al.*[27] presented an identification algorithm using DOB by applying an orthogonal condition to decouple the inertia term from the motion response. In the proposed method the authors initially obtained the inertia, calculated the viscous coefficient based on the inertia, and finally calculated the constant applied force. Since the three parameters are not evaluated simultaneously, the error in the estimate of one parameter affects another. Restated, the viscous friction, the Coulomb friction and other unknown position-dependent forces influence the evaluation of inertia. A biased estimate of inertia will in turn affect the accuracies of the estimates of the viscous coefficient and the Coulomb friction. Additionally, the approach in[27] requires the controller to be tuned according to the evaluated parameters, and several experimental tests to be performed and still does not guarantee convergence to nominal values.

This work presents a new algorithm that can evaluate the three parameters in a single motion test. The rest of this paper is organized as follows. The following section describes the experimental system. Section 3 discusses in detail the experimental methods required for the advanced parameter identification of a linear-motor-driven motion system. Section 4 compares the simulated and experimental results obtained using different identification methods. Section 5 draws conclusions.

2. Experimental System

2.1 Hardware setup

The experimental motion system, presented in Fig. 1, has the following components: a linear-motor-driven motion system, a laser displacement meter, and a PC (PC1 in Fig. 1) with a DAC and encoder interface. The linear motor system has a linear motor (IL6-050A1) and an AC servo amplifier (SERVOSTAR CD) operating in torque (current) mode, both of which were obtained from the Kollmorgen Corporation.[28] Two sensors were used in this system - one with a linear scale (RENISHAW RGH24Y, resolution 0.1 micrometer) to provide position information for the vector control of the servo amplifier, and a fiber optic laser encoder (RENISHAW RLE10) to measure the displacement of the motion table with an adjustable resolution. The accuracy of the resolution supplied by RLE10 is influenced by such environmental effects as relative humidity, temperature, pressure and cosine errors. Hence, calibration must be performed using another measurement instrument. The RENISHAW laser interferometer system which includes an environmental compensation unit (EC10) was adopted. Following calibration, the basic length units (BLU) for coarse and fine resolutions were found to be 0.0791 μm and 0.020 μm, respectively. The selection of the resolution scale depends on the encoder transition time (1 MHz in our system), the desired maximum velocity, and the travel range. The velocity was estimated from the fiber optic laser encoder using an $\alpha\beta$ -filter[29] in the motion system.

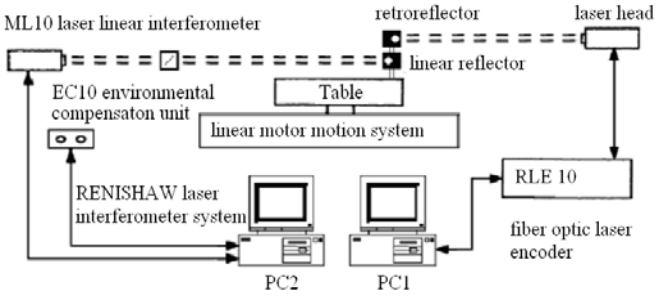

Fig. 1 Experimental linear-motor-driven motion system and the resolution calibration system

2.2 Model of the mechanical system

The bandwidth of current loop is much higher than that of the mechanical system. If the high-frequency modes are ignored, then the system equation can be simplified to

$$J\ddot{x} + B\dot{x} + F_1 = u \tag{1}$$

where J denotes the inertia (equivalent mass); $B\dot{x} + F_1$ is the friction force, and u is the force input to the system generated by a current-controlled servo amplifier with a velocity loop controller and a position loop controller. The damping coefficient is regarded as a parameter of the controlled plant herein. Therefore, F_1 represents a friction force without a viscous friction term. F_1 is generally a function of position, velocity and control input force.

3. Parameters Identification of the Linear-Motor Stage

The DOB is proposed in a system to reduce the effort required to obtain a highly accurate system model. The internal loop compensator formed by the DOB can generate corrective control inputs to reject as much of the equivalent disturbance as possible, so to force the actual system to become a given nominal model. The equivalent disturbance consists of a real external disturbance and an extra force to eliminate the model uncertainty. The internal loop compensator may become unstable if the control input is saturated because of large plant uncertainty.[30]

Figure 2 presents block diagrams of the disturbance observer; Fig. 2(a) presents the original structure. In Fig. 2(b), a low-pass filter is adopted to yield an implementable strictly proper rational function. The output of DOB is an estimate of disturbance, which can be used for compensation. However, the DOB herein is used for parameter identification. The symbols are defined as follows.

$v(s)$: the velocity response of motion table

$\zeta(s)$: the measurement noise or error in estimated velocity

$P(s)\left(=\dfrac{1}{Js+B}\right)$: the transfer function of plant

$P_n(s)\left(=\dfrac{1}{J_n s+B_n}\right)$: the desired transfer function of plant

$u(s)$: the control input

$d(s)$: the disturbance, including friction and external forces

$Q(s)$: a low-pass filter

$\tau(s)$: the estimated disturbance without filtering

$\hat{\tau}(s)$: the value of estimated disturbance with a low-pass filter

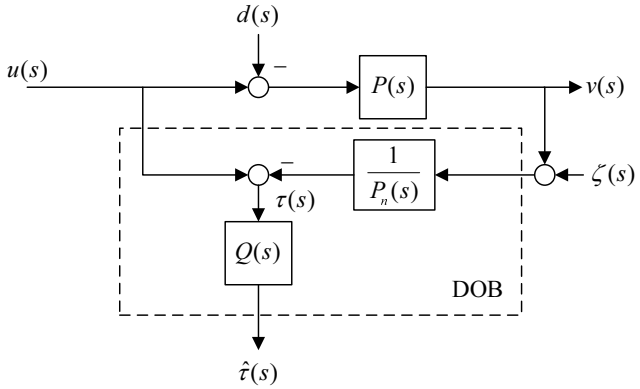

(a) Original structure

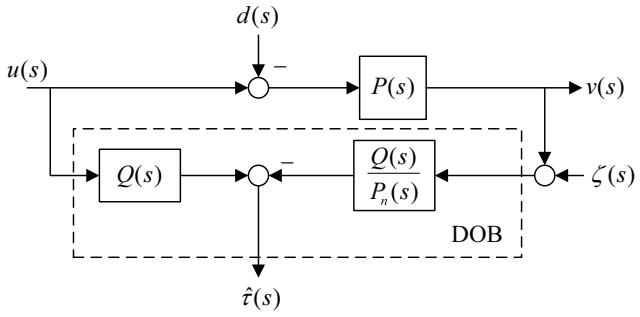

(b) Structure for implementation

Fig. 2 Block diagrams of disturbance observers

Ignore the low-pass filter $Q(s)$. From Fig. 2(a), the following relations can be derived;

$$\tau(s)=u(s)-\frac{1}{P_n(s)}\big(v(s)+\zeta(s)\big) \tag{2}$$

Substituting $P_n(s)=\dfrac{1}{J_n s+B_n}$ into the above equation yields

$$\tau=u-J_n\dot{v}-B_n v-\left(J_n\dot{\zeta}+B_n\zeta\right) \tag{3}$$

Similarly, $u(s)-d(s)=\dfrac{1}{P(s)}v(s)$ and $P(s)=\dfrac{1}{Js+B}$, yielding

$$u=d+J\dot{v}+Bv \tag{4}$$

Therefore,

$$\begin{aligned}\tau&=d+J\dot{v}+Bv-J_n\dot{v}-B_n v-\left(J_n\dot{\zeta}+B_n\zeta\right)\\&=d+\Delta J\dot{v}+\Delta Bv-\left(J_n\dot{\zeta}+B_n\zeta\right)\end{aligned} \tag{5}$$

where $J=J_n+\Delta J,\ \ B=B_n+\Delta B.$

If no measurement noise or modeling error is involved, such that $J=J_n$ and $B=B_n$, then the real external disturbance d can be estimated perfectly. In Fig. 2(a), the relationship between the unfiltered signal τ and the real estimate of the equivalent disturbance $\hat{\tau}$ is defined as follows.

$$\hat{\tau}=Q(s)\tau \tag{6}$$

The choice of $Q(s)$ for control is to let the low-frequency dynamics of $Q(s)$ be close to 1 for disturbance and model uncertainties rejection. The high-frequency dynamics must be close to 0 for sensor noise rejection. The order of $Q(s)$ is determined considering the rational proper property of $\dfrac{Q(s)}{P_n(s)}$. Umeno and Hori[12] and Lee and Tomizuka[13] proposed some forms of $Q(s)$ filters. In this work, a second-order filter which exhibits the above stated properties is selected as

$$Q(s)=\frac{1}{(qs+1)^2}\quad=\frac{1}{q^2s^2+2qs+1} \tag{7}$$

where q is the time constant of the filter. Notably, $|Q(s)|\approx 1$ for frequencies under $1/q$, and $|Q(s)|$ rolls off at -40 dB/decade for frequencies over $1/q$. The active frequency range of DOB is inversely proportional to q. For control, the magnitude of q represents a compromise between the desired active dynamic range and the measurement noise. A larger q corresponds to a smaller bandwidth of a low-pass filter, $Q(s)$, and a less robust system. Choi *et al.*[30] recommended that q should be 10 to 15 times the sampling time. For identification, q can be easily decided. The frequencies of the disturbance are typically low. The bandwidth of the open-loop system is also low. The cutoff frequency of $Q(s)$ can be chosen to exceed slightly the maximum of the frequency of velocity command, the frequency of the disturbance and the bandwidth of the system plant. Although the latter two frequencies are not exactly known, a rough estimate can be made according to the system configuration and the operating conditions. In this work, 5 Hz is set as the cutoff frequency of $Q(s)$. This low pass filter can reduce most of the measurement noise while preserving the required signal.

If the table is not at an incline, the gravitational force can be neglected. Furthermore, based on the assumption that the friction, F_1, is the only disturbance one is interested in, the equivalent disturbance is obtained from Eqs. (5)-(6) as follows.

$$\hat{\tau}=Q\Big(d+\Delta J\dot{v}+\Delta Bv-\left(J_n\dot{\zeta}+B_n\zeta\right)\Big)\cong F_1+\Delta J\dot{v}+\Delta Bv+\delta \tag{8}$$

where δ consists of equivalent forces associated with measurement noise, cogging force, torque ripples, servo lag and other factors. The drop in the order of the plant model also introduces some equivalent forces. A new method based on the orthogonal relation is proposed below. It yields reasonable estimates of system inertia, the viscous coefficient, and the Coulomb friction force. The parameters can be estimated in both positive and negative directions. For positive direction, the system parameters can be estimated with the velocity command:

$$v_r(t) = v_0 + v_1 \sin\left(\frac{2\pi}{T_p}t\right) \tag{9}$$

Its corresponding acceleration profile will be

$$\dot{v}_r(t) = v_1 \frac{2\pi}{T_p}\cos\left(\frac{2\pi}{T_p}t\right) \tag{10}$$

where $v_0 > v_1 > 0$ and T_p is the period of this sinusoidal function.

The chosen v_r should not be too close to zero to avoid nonlinear effects around zero velocity, such as stiction and the Stribeck effect. The motion is designed to be a unidirectional motion without velocity reversal. If the Stribeck velocity, v_s, is already known from some other experiment, a better relationship between v_0 and v_1 can be given as

$$v_0 - v_1 > v_s \tag{11}$$

When the table slides at above the Stribeck velocity, v_s, the friction force is reduced to the Coulomb friction, i.e., $F_1 = F_C$. For parameter identification, the frequency component of applied velocity command is quite low; therefore, the system response will be assumed to catch up with the command easily after a short time if the PI velocity controller is tuned properly. Moreover, since the velocity and acceleration response are all sinusoidal functions, the orthogonal relations can be employed to decouple different components associated with the error estimates of different parameters. Notably, the transitional response data at the start of motion are not suitable for identification because the tracking error is large. A suitable range of steady-state signals over a period T_p should be carefully chosen to meet the orthogonal conditions. Multiplying (8) by $\dot{v}$ and integrating the result over a chosen period T_p, yields Eq. (12).

$$\int_{T_p}(\hat{\tau}\dot{v})\,dt = \int_{T_p}(\Delta J\,\dot{v}\dot{v})\,dt + \int_{T_p}(\Delta B\,v\dot{v})\,dt + \int_{T_p}(F_C\,\dot{v})\,dt + \int_{T_p}(\delta\,\dot{v})\,dt \tag{12}$$

From the following orthogonal relations and trigonometric properties,

$$\int_{T_p}(\Delta B\,v\dot{v})\,dt = 0 \tag{13}$$

and

$$\int_{T_p}(F_C\,\dot{v})\,dt = 0 \tag{14}$$

Assume that the following equation is true,

$$\int_{T_p}(\delta\,\dot{v})dt \approx 0 \tag{15}$$

Then the estimated error of the inertia parameter is

$$\Delta J = \frac{\int_{T_p}(\hat{\tau}\dot{v})\,dt}{\int_{T_p}(\dot{v})^2\,dt} \approx \frac{\sum_{k=1}^{k=N}\hat{\tau}[k]\dot{v}[k]\,T}{\sum_{k=1}^{k=N}\dot{v}^2[k]\,T} = \frac{\sum_{N}\hat{\tau}[k]\dot{v}[k]}{\sum_{N}\dot{v}^2[k]} \tag{16}$$

where N denotes the sampling number over a period and T is the sampling time. Mathematically, the accuracy of the integration can be improved by increasing N or decreasing T. An updated value of inertia can be obtained using the following equation:

$$\hat{J}_{new} = \hat{J}_{old} + \Delta J \tag{17}$$

One problem remains here. The measured noise will be amplified when the acceleration and velocity are estimated by differentiating the position data. Furthermore, in our system, the resolution of the fiber optic laser encoder (RENISHAW RLE10) is 0.0791 μm and the sampling rate is 2 kHz. One pulse error between two consecutive measured positions will induce the minimum acceleration error of 316.4 mm/s^2 due to the double differentiation from the measured data. For instance, when the velocity command is $v_r = 40 + 30\sin(5t)$ *mm/s*, the theoretic acceleration is $150\cos(5t)$ mm/s^2, which is less than the acceleration resolution. As for the velocity, although the minimum estimated velocity error 1.582×10^{-1} mm/s is not large when compared with the velocity command, the estimated velocity also suffers noise problem. As a solution to the problem, the frequency of the command is chosen to be less than 1 Hz so that the system response can catch up the command easily using the tuned PI velocity controller while the system bandwidth is around 60Hz in our simulation and experiment. Therefore, both the reference velocity v_r and reference acceleration $\dot{v}_r$ are adopted in our identification processes, based on the assumption that if $v = v_r$ is true, then $\dot{v} = \dot{v}_r$ will also be true.

Extend the similar operation to estimate the viscous coefficient B. Multiplying (8) with v and integrating it over a chosen period, T_p, one get (18).

$$\int_{T_p}(\hat{\tau}v)\,dt = \int_{T_p}(\Delta J\,\dot{v}v)\,dt + \int_{T_p}(\Delta B\,vv)\,dt + \int_{T_p}(F_C\,v)\,dt + \int_{T_p}(\delta\,v)\,dt \tag{18}$$

Since v and v_r are sinusoidal functions with a constant offset, the first term in the right-hand side of the above equation is zero due to the orthogonal relations, that is,

$$\int_{T_p}(\Delta J\,\dot{v}v)\,dt = 0 \tag{19}$$

Since

$$\begin{aligned}\int_{T_p}(F_C\,v)\,dt &= \int_{T_p}(F_C\,v_0)\,dt + \int_{T_p}(F_C\,v_1\sin(\frac{2\pi}{T_p}))\,dt \\ &= F_C v_0 T_p \\ &\neq 0\end{aligned} \tag{20}$$

and assume that the following equation is true;

$$\int_{T_p}(\delta\,v)dt = \int_{T_p}(\delta\,v_0)dt + \int_{T_p}\left(\delta\,v_1\sin(\frac{2\pi}{T_p})\right)dt \approx 0 \tag{21}$$

from Eq. (18) the estimated error of B is given by Eq. (22).

$$\left.\begin{aligned}\Delta B &\approx \frac{\int_{T_p}(\hat{\tau}\,v)dt - \int_{T_p}(F_C\,v)dt}{\int_{T_p} v^2 dt} \\ &\approx \frac{\sum_{k=1}^{k=N}\hat{\tau}[k]v[k]\,T - F_C\sum_{k=1}^{k=N}v[k]T}{\sum_{k=1}^{k=N}v^2[k]\,T} \\ &= \frac{\sum_{N}\hat{\tau}[k]v[k] - F_C\sum_{N}v[k]}{\sum_{N}v^2[k]}\end{aligned}\right\} \quad (22)$$

If F_C is known, then an updated viscous coefficient is given by the following equation

$$\hat{B}_{new} = \hat{B}_{old} + \Delta B \quad (23)$$

Of course, the Coulomb friction F_C and the viscous coefficient B can be obtained by performing other experiments, such as those experiments performed elsewhere to plot friction-velocity map. However, these experiments are quite time-consuming and they are unable to estimate the important inertia parameter. It does not matter whether the friction-velocity map is constructed experimentally or not, this proposed method yields the best solution for the three parameters from the viewpoint of signal decomposition. Furthermore, this method can estimate three parameters from just one set of measured data.

The key to solving Eq. (22) is to estimate the value of F_C first. Rewrite (8) as follows

$$\hat{\tau} = F_C + \Delta J\dot{v} + \Delta B v + \delta \quad (24)$$

Some facts are known about the right-hand side of the above equation: a) F_C is a constant; b) $\Delta J\dot{v}$ is a pure sinusoidal function with zero offset, and c) ΔBv is a sinusoidal function with a constant offset. The mean values of all $\hat{\tau}$ sampled over the period T_p yields the following equation,

$$\left.\begin{aligned}\hat{F}_C &= \frac{1}{N}\sum_{k=1}^{k=N}\hat{\tau}[k] \\ &= \frac{1}{N}\sum_{N}\hat{\tau}[k]\end{aligned}\right\} \quad (25)$$

$\hat{F}_C$ is the estimate of F_C. It can be further evaluated as follows,

$$\begin{aligned}\hat{F}_C &= \frac{1}{N}\Delta J\sum_{k=1}^{k=N}\dot{v}[k] + \frac{1}{N}\Delta B\sum_{k=1}^{k=N}v[k] + F_C + \frac{1}{N}\sum_{k=1}^{k=N}\delta[k] \\ &= \Delta B\,v_0 + \frac{1}{N}\sum_{N}\delta[k] + F_C\end{aligned} \quad (26)$$

N is the number of sampled points over a period. Again, if the noise-related term is zero, such that

$$\frac{1}{N}\sum_{N}\delta[k] \approx 0 \quad (27)$$

then $\hat{F}_C$ will converge. If $\Delta B = 0$ is true, then $\hat{F}_C = F_C$ will be true.

Clearly, a large N helps to yield an accurate estimate of F_C. Averaging the data over several periods is a way to increase the number N. Increasing the sampling rate is another effective method. However, some physical limitations, such as travel length and the memory size of the computer, constrain the sampled number N. Since the estimate of $\hat{F}_C$ exhibits the large sample property, the estimator defined by Eq. (25) is a consistent estimator. Notably, however, the above three parameter estimators are all biased estimators, unless the expectation of the term δ is zero. During the identification process, the errors ΔB and ΔJ in the parameters converge toward zero following several iterations. In the meantime, the value of F_C converges to $\hat{F}_C$. If B and F_C are not updated iteratively, the estimate of J will become more seriously biased because of the degradation of the orthogonal conditions caused by the larger tracking error. Likewise, an erroneous estimate of J degrades the estimates of B and F_C.

From the above discussions, the following steps are proposed to estimate three system parameters.

Step 1: Perform a velocity tracking control experiment. The reference command must look like Eq. (9) and be unidirectional. Figure 3 presents the proposed control structure, in which the PI controller must be tuned to uphold the assumptions of $v = v_r$ and $\dot{v} = \dot{v}_r$. The notations K_a and K_t are the gain of current driver and the force constant of motor, respectively, and these two coefficients are generally constant values.[25]

Step 2: Calculate ΔJ using the following equation.

$$\Delta J = \frac{\sum_{N}\hat{\tau}[k]\dot{v}_r[k]}{\sum_{N}\dot{v}_r{}^2[k]} \quad (28)$$

Step 3: Update the estimate of inertia.

$$\hat{J}_{new} = \hat{J}_{old} + \Delta J \quad (29)$$

Step 4: Estimate the Coulomb friction F_C.

$$\hat{F}_C = \frac{1}{N}\sum_{N}\hat{\tau}[k] \quad (30)$$

Step 5: Calculate ΔB using the following equation.

$$\Delta B = \frac{\sum_{N}\hat{\tau}[k]v_r[k] - \hat{F}_C\sum_{N}v_r[k]}{\sum_{N}v_r{}^2[k]} \quad (31)$$

Step 6: Update the viscous coefficient B.

$$\hat{B}_{new} = \hat{B}_{old} + \Delta B \quad (32)$$

Step 7: Refresh the updated $\hat{J}_{new}$ and $\hat{B}_{new}$ in $P_n(s)$ of DOB. The experimental control input $u(s)$ and the estimated velocity v are fed into the new DOB to yield a new series of disturbance estimates $\hat{\tau}$. Then return to step 2 to perform next estimation. If ΔJ and ΔB are almost zero by satisfying the convergent conditions, then stop. When the following errors are considered, that is, $v \neq v_r$ and $\dot{v} \neq \dot{v}_r$,

one shows the convergence condition of the iterative process in the Appendix.

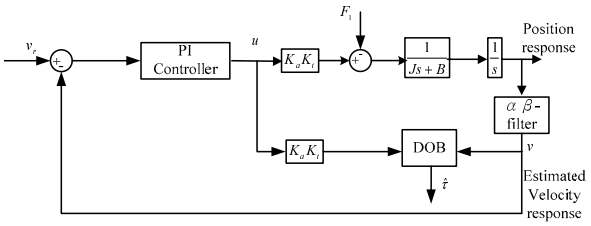

Fig. 3 Block diagrams of proposed identification experiment

3.1 Discussion and simulation

In one experimental test, the estimate of the three parameters is repeated several times until a final steady state is reached. If the tracking error is made small by tuning the PI controller, one experiment is enough to estimate these three parameters. Otherwise, the new estimates can be used to redesign the controller for improving the tracking performance, and also as the initial values in another motion control test.

Three simulations are performed to demonstrate the effectiveness of the proposed method with different initial values. Notably, the 14-bit D/A quantization effect and ±4 BLU measured noise (1 BLU=0.0791μm, uniform distribution) are included in the simulation. The reference command is defined as

$$v_r = 30 + 20\sin(5t) \ \text{mm/s}$$

Table 1 lists the nominal, initial and final values for each simulation. All simulations almost come to the same results. Figure 4 draws the results of simulation I which indicates good parameter convergence. Therefore, it is concluded that the parameters can converge to the actual ones with different initial values in the proposed identification process. In addition, a method proposed elsewhere[27] is used for comparison. In the reference method, the whole system might be unstable due to improper initial value of the equivalent inertia, such as $J = 0\ kg$. Figure 5 draws the simulations where the initial values in our proposed method are zero and Table 2 presents the values of the parameters used in the simulations and the final values obtained by the two methods. Our estimated parameters can reach the nominal value with accuracy smaller than 1% after 10 iterations. In short, the proposed method is clearly superior. The convergence is very fast, and the values obtained by convergence are more accurate than those obtained using the reference method. The proposed method requires only one experiment to be performed to identify the three parameters, while the method from the literature depends on more experiments, and still does not guarantee convergence to nominal values.

Table 1 Three simulations with different initial values using the proposed method

Parameter	Nominal Value	Simulation I		Simulation II		Simulation III	
		Initial value	Final value	Initial value	Final value	Initial value	Final value
J(kg)	10.0	20	9.942	15	9.944	6	9.943
B(kg/s)	110.0	50	109.798	80	109.811	20	109.802
F_C (N)	7.0	10	7.005	3.0	7.004	5	7.005

Table 2 Comparisons based on simulation using the proposed method and the method from the literature after ten iterations

Parameter	Nominal value	Proposed method		
		Initial value P_N	Final value P_{E1}	Estimated Accuracy $\frac{\lvert P_{E1}-P_N\rvert}{P_N}\%$
J(kg)	10.0	0.0	9.94	0.60%
B(kg/sec)	110.0	0.0	109.8	0.18%
F_C (N)	7.0	0.0	7.0	0.00%
		Reference method		
		Initial value P_N	Final value P_{E2}	Estimated accuracy $\frac{\lvert P_{E2}-P_N\rvert}{P_N}\%$
		3.0	9.93	0.70%
		50.0	121.0	10.00%
		0.0	8.1	15.71%

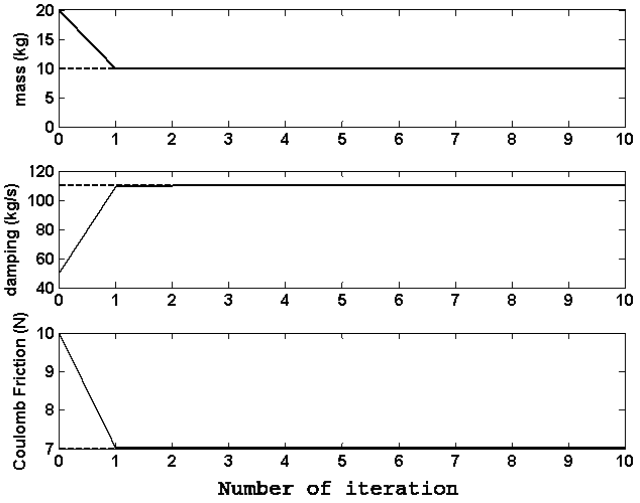

Fig. 4 Results of Simulation I with initial values listed in Table 1

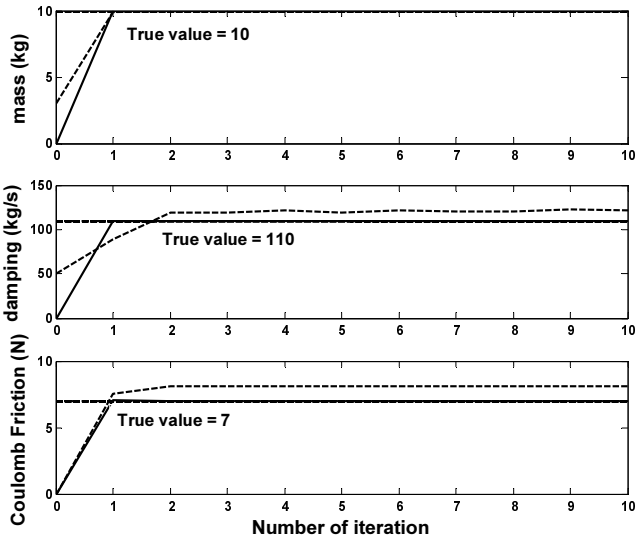

Fig. 5 Identification performed using the method in the literature (dashed line) and the proposed method (solid line)

4. Experiment Results

Figures 6-8 refer to an experimental study of the evaluation of parameters. The designed velocity command is

$$v_r = 40 + 30\sin(5t) \text{ mm/s}$$

A period between 0.314s and 1.57s is chosen with a sampling interval of 0.005s for parameter estimation, to avoid the transition near the motion-start region. Figure 6 presents the initial estimate of the equivalent disturbances $\hat{\tau}$ and the control forces. Since all initial parameters are set to zero, this equivalent disturbance is simply a filtered control force. Figure 7 presents the final estimate of the equivalent disturbance and the control force after 20 iterations. The equivalent disturbances in Figs. 6 and 7 reveal that the original bowl-shaped disturbance becomes almost flat with a small variation, indicating that the parameter uncertainties are reduced. The mean value of the final equivalent disturbance is the Coulomb friction and the variation part is related to the term δ. The normalized parameter error indices are defined as:

$$C_J = \frac{|\Delta J|}{J}, \quad C_B = \frac{|\Delta B|}{B}$$

with the convergent conditions (C_J < 0.05) and (C_B <0.05).

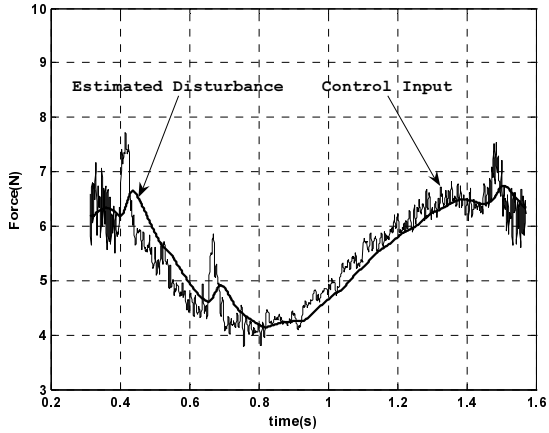

Fig. 6 Initial estimate of equivalent disturbance and measured control force in the chosen period

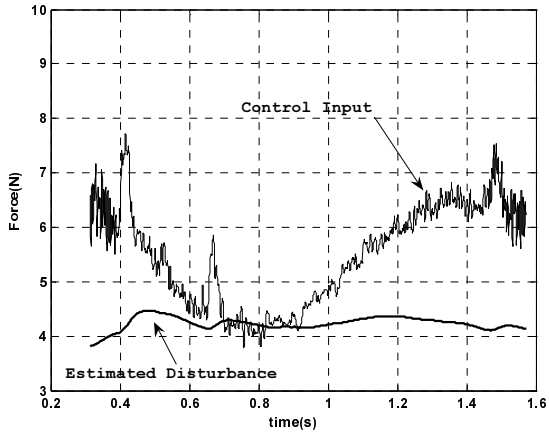

Fig. 7 Equivalent disturbance and measured control force in the chosen period after 20 iterations

Figure 8 displays five experimental results, to demonstrate the repeatability of the proposed method; and it takes at most 17 iterations for each experiment to obtain the convergent estimated parameters. The mean values of estimated parameters are $J = 4.46$ kg, $B = 24.03$ kg/s, and $F_C = 4.29$N. All the parameters of the motion system including the estimated parameters, *J*, *B*, and F_c are listed in Table 3.

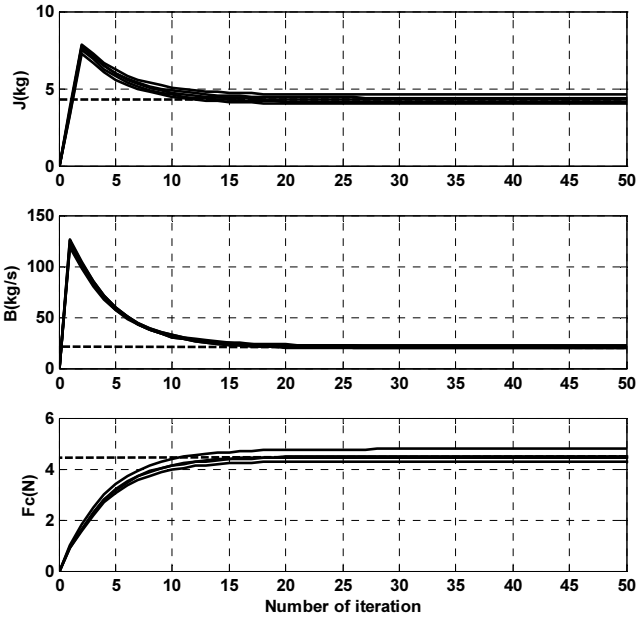

Fig. 8 The three parameters converge to their final values after 50 iterative estimations (in five experiments)

Table 3 Parameters of experimental system

Symbol and name	Value	Unit
J, inertia	4.46	kg
B, viscous friction coefficient	24.03	kg/s
F_C, Coulomb friction force	4.29	N
K_t, force constant of motor	28.5	N/A
K_a, gain of current driver	0.349	A/V
T, sampling rate	0.0005	s
D, pole-pitch of motor	32	mm

More simulations and experiments are conducted to further validate the estimated parameters from both frequency-domain and time-domain point of view. Figures 9-10 show the block diagrams of motion system with and without Coulomb friction model, respectively. The model in Fig. 9 is used for simulation I, while the model in Fig. 10 is for simulations II and III listed in Table 4.

A conventional experiment is conducted to obtain system parameters *J* and *B* by the step response method for comparison. A 1.5 V step force command is used and the parameters, $J = 6.74$ kg and $B = 28.69$ kg/s, obtained. The frequency response of the motion system - the linearized system - is measured as a base line of a peak-to-valley 4 V swept sin experiment over a frequency range from 0.3Hz to 10Hz using the dynamic signal analyzer, HP 35665A. The solid line in Fig. 11 plots the experimental frequency

response and is used to verify the fit of the following three sets of simulation results. Table 4 presents the system model, the identification algorithm, the identified parameters and the poles of the linearized system at low frequency for the experimental system and each simulation system. Notably, the fifth column in Table 4 represents the locations of the pole and zero in each case, using the function INVFREQS in Matlab. Figure 11 also presents the frequency responses for the three simulation results. The plot of simulation I (dashed-line) is obtained from the swept sin simulation with frequency range from 0.3Hz to 10Hz to the system shown in Fig. 9. Figure 12 presents the typical time responses of the experimental and simulated (I) results using 2Hz sinusoidal command. Since the underlying system with friction is nonlinear, the velocity response is not a perfect sinusoid. The frequency response is calculated from the magnitude and the phase of the first harmonic of the input force and the velocity response.

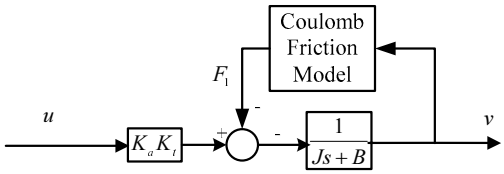

Fig. 9 Block diagram of motion system with Coulomb friction model for simulation I

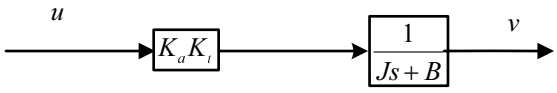

Fig. 10 Block diagram of motion system without Coulomb friction model for simulations II and simulation III

As presented in Fig. 11, the simulated (I) almost fits the experimental response, implying that our identified algorithm can obtain the system parameters accurately. The simulated (II) (dotted line) is performed using the system shown in Fig. 10 with parameters listed in Table 4. Comparing the experimental and simulated (II) frequency response plots reveals that the magnitude of the latter response is close to the real value at frequencies of under 0.7 Hz and deviates from the real value at higher values. In

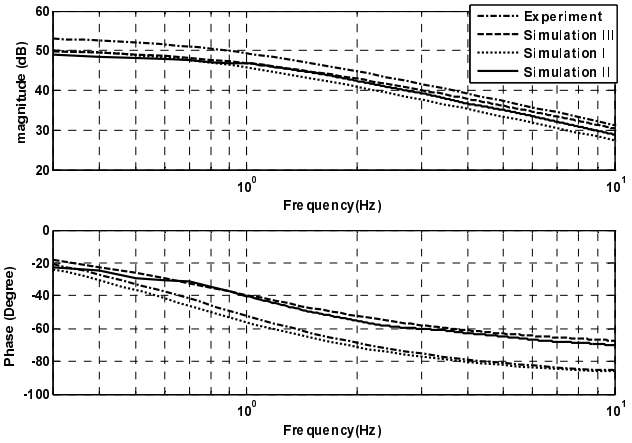

Fig. 11 Experimental and simulated frequency responses in peak-to-valley 4 V swept sin tests. Table 4 provides the conditions of experimental and simulation systems

the meantime, the phase decreases more rapidly than that of the real system. As shown in the fifth column in Table 4, the pole of the linearized underlying system in the low frequency range is at -6.31 and exceeds the pole in simulated (II) at -4.26. Therefore, the simulated (II) cut-off frequency is smaller than the real value. Furthermore, if the system parameters in the simulation II are identified from our proposed method without taking the Coulomb friction parameter into account, frequency response in simulation III is as presented by the dashed-dotted line in Fig. 11. The magnitude of the response exceeds the real values because the DC-gain in simulation III system exceeds the real system. The pole in simulation III system is close to that in simulation II and the phase response of the simulation III is similar to that in the simulation II. Other swept sin experiments with peak-to-valley amplitudes of 8 V and 10 V are performed, and similar results are obtained. In summary, the proposed method can catch the main features of the system from the frequency-domain aspect.

In the time-domain, a 0.8 V step force command, presented in Fig. 13(a), is used to evaluate the time responses of the above three simulation systems, listed in Table 4. The solid line in Fig. 13(b) plots the experimental results of the motion system. The results reveal that time response of the simulated (I) almost matches that of

Table 4 Condition of the experiment and simulated systems

	System	Identification method	Identified Parameters	Poles (at low frequency range) and DC gain of the linearized system
Experiment	Shown in Fig. 1	Swept sin from HP 35665A	None	For 4 poles, no zero Pole= -6.31 DC gain= 296.33
Simulation I (dashed-line)	Shown in Fig. 9 $\frac{1}{Js+B}$ and F_C	Proposed Method	J=4.46 kg, B=24.03 kg/s, F_C =4.29 N.	For 4 poles, no zero Pole= -6.76 DC gain= 306.60
Simulation II (dotted-line)	Shown in Fig. 10 with $\frac{1}{Js+B}$	Step response method	J=6.74 kg B=28.69 kg/s.	Pole= -4.26 DC gain= 346.70
Simulation III (dashed-dotted line)	Shown in Fig. 10 with $\frac{1}{Js+B}$ and no F_C	Proposed Method	J=4.46 kg, B=24.03 kg/s	Pole= -5.39 DC gain=413.92

the real system, except when the command changes abruptly.

Meanwhile, the simulated time responses in simulations II and III have a larger magnitude than the real response.

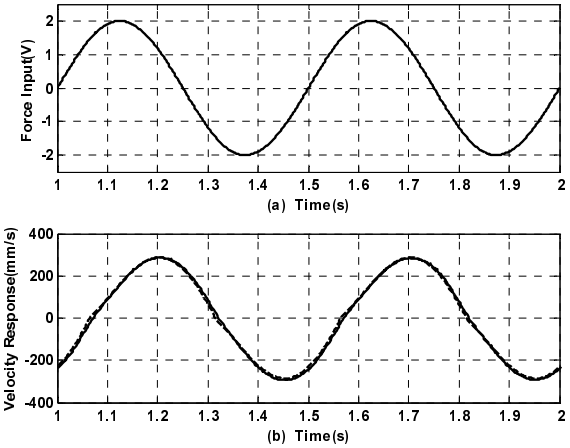

Fig. 12 2Hz sinusoidal velocity command and associated experimental (solid line) and simulated (I) results (dashed line)

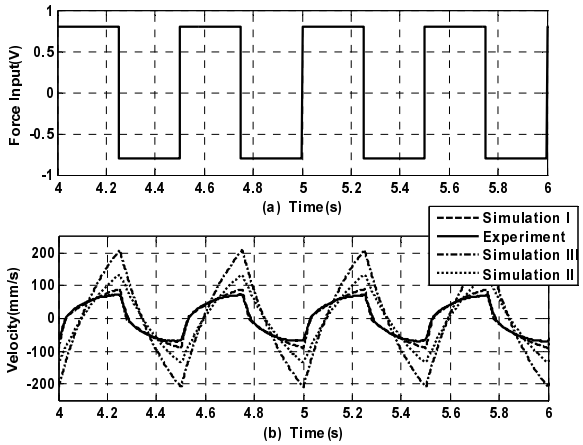

Fig. 13 Experimental and simulated (a) force input and (b) velocity response results. Table 4 provides the conditions of experimental and simulation systems

4.1 Application

In the following experiments, the control configuration shown in Fig. 14, including a velocity P-controller (P), and the disturbance observer compensator (DOB) with a 10 Hz bandwidth, is designed for the underlying linear-motor-system with a 30Hz closed-loop bandwidth. The frequency response of the closed-loop system is measured from the swept sin test in a frequency range from 0.1Hz to 100Hz. As displayed in Fig. 15(a), the experimental bandwidth is 34Hz, which is close to the desired control bandwidth, 30 Hz. If an extra mass 3.72Kg is mounted on the linear motor table, the experimental frequency response becomes worse as the bandwidth becomes 18Hz, as shown in Fig. 15(b). Figure 15(c) demonstrates that the performance at a bandwidth of 32Hz is recovered under the extra-inertia condition, if the system parameters are identified again by our proposed method and the controller gains are redesigned. Notably, the identification algorithm and the control algorithm are implemented digitally. Hence, the servo loop supports auto-tuning.

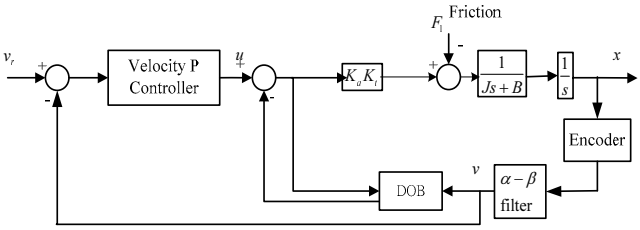

Fig. 14 Controller configuration (P+DOB) in the experiment

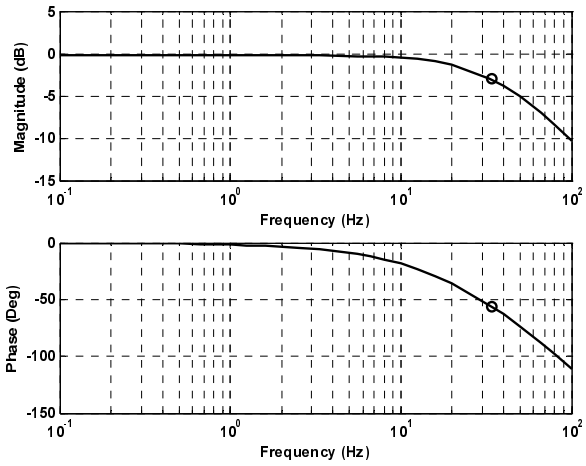

(a) Original system with the initial controller gains

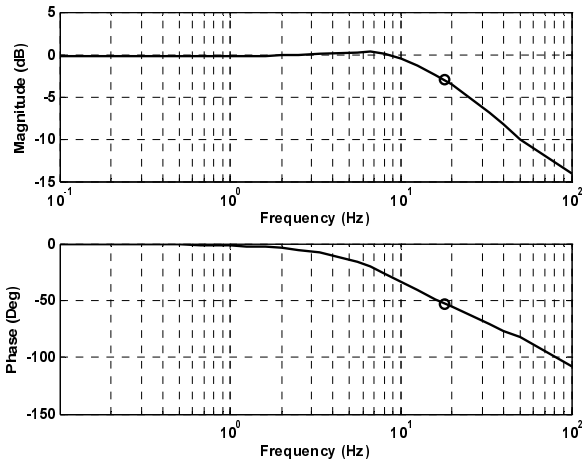

(b) System with extra mass and initial controller gains

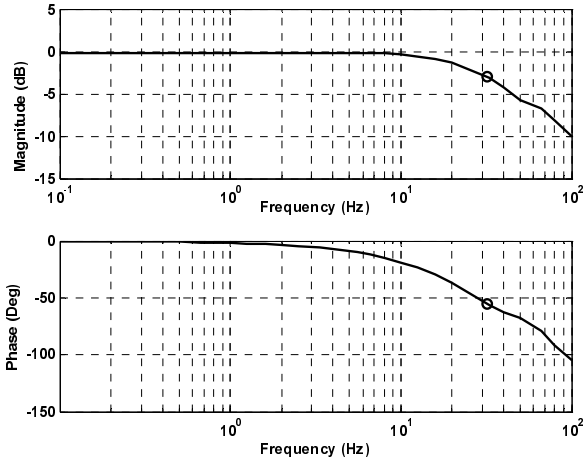

(c) System with extra mass and renewed controller gains

Fig. 15 Frequency responses for each closed loop system

5. Conclusion

This work demonstrated the effectiveness of an advanced identification procedures for a linear motor motion system. An efficient algorithm for estimating inertia, viscous coefficient and Coulomb friction is presented using DOB. These three parameters can be identified iteratively based on the orthogonal relationships and trigonometric properties among parameters and comments. Simulation and experimental results successfully validated our proposed algorithm, and the algorithm can be implemented digitally to enhance the control performance. Further study will be conducted to improve the current method by including those predictable disturbances such as the force ripple, cogging force in the motion system.

ACKNOWLEDGEMENTS

The authors would like to thank the National Science Council of the Republic of China for financially supporting this paper under contract No. NSC92-2212-E-009-018.

REFERENCES

1. Tanaka, T., Ikeda, K., Otsuka, J., Masuda, I. and Oiwa, T., "Influence of Rolling Friction in Linear Ball Guideways on Positioning Accuracy," Int. J. of Precision Engineering and Manufacturing, Vol. 8, No. 2, pp. 85-89, 2007.
2. Horng, R. H., Lin, L. R. and Lee, A. C., "LuGre Model-Based Neural Network Friction Compensator in a Linear Motor Stage," Int. J. of Precision Engineering and Manufacturing, Vol. 7, No. 2, pp. 18-24, 2006.
3. Ljung, L., "System Identification: Theory for the User," Prentice-Hall, Inc., pp. 274-282, 1987.
4. Spetch, R. and Isermann, R., "On-line Identification of Inertia, Friction and Gravitational Forces Applied to an Industrial Robot," Proc. IFAC Symp. on Robot Control, SYROCO'88, pp. 88.1-88.6, 1988.
5. Held, V. and Maron, C., "Estimation of Friction Characteristics, Inertial and Coupling Coefficients in Robotic Joints Based on Current and Speed Measurements," Proc. IFAC Symp. on Robot Control, SYROCO'88, pp. 86.1-86.6, 1988.
6. Chang, L. H. and Lee, A. C., "Design of Nonlinear Controller for Bi-axial Inverted Pendulum System," IET Control Theory and Applications, Vol. 1, No. 4, pp. 979-986, 2007.
7. Kim, N. J., Moon, H. S. and Hyun, D. S., "Inertial Identification for the Speed Observer of the Low Speed Control of Induction Machines," IEEE Trans. on Industry Applications, Vol. 32, No. 6, pp. 1371-1379, 1996.
8. Hong, S. J., Kim, H. W. and Sul, S. K., "A Novel Inertia Identification Method for Speed Control of Electric Machine," Proc. IECON, pp. 1234-1239, 1996.
9. Choi, J. W., Lee, S. C. and Kim, H. G., "Inertia Identification Algorithm for High-performance Speed Control of Electric Motors," IEE Proc. of Electric Power Applications, Vol. 153, No. 3, pp. 379-386, 2006.
10. Kim, K. H., "Nonlinear Speed Control for a PM Synchronous Motor with a Sequential Parameter Auto-tuning Algorithm," IEE Proc. Control Theory Applications, Vol. 152, No. 5, pp. 1253-1262, 2005.
11. Ohnishi, K., "A New Servo Method in Mechatronics," Trans. IEEJ Industrial Application, Vol. 107-D, pp. 83-86, 1987.
12. Umeno, T. and Hori, Y., "Robust Speed Control of DC Servomotors Using Modern Two Degree-of-freedom Controller Design," IEEE Trans. on Industrial Electronics, Vol. 38, No. 5, pp. 363-368, 1991.
13. Lee, H. S. and Tomizuka, M., "Robust Motion Controller Design for High-accuracy Positioning Systems," IEEE Trans. on Industrial Electronics, Vol. 43, No. 1, pp. 48-55, 1996.
14. Komada, S., Machii, N. and Hori, T., "Control of redundant manipulators considering order of disturbance observer," IEEE Trans. on Industrial Electronics, Vol. 47, No. 2, pp. 413-420, 2000.
15. White, M. T., Tomizuka, M. and Smith, C., "Improved Track Following in Magnetic Disk Drives Using a Disturbance Observer," IEEE/ASME Trans. on Mechanics, Vol. 5, No. 1, pp. 3-11, 2000.
16. Shahruz, S. M., "Performance Enhancement of a Class of Nonlinear Systems by Disturbance Observers," IEEE/ASME Trans. on Mechanics, Vol. 5, No. 3, pp. 319-323, 2000.
17. Iwasaki, M., Shibata, T. and Matsui, N., "Disturbance-observer-based Nonlinear Friction Compensation in Table Drive System," IEEE/ASME Trans. on Mechatronics, Vol. 4, No. 1, pp. 3-8, 1999.
18. Horng, R. H., Chou, H. L. and Lee, A. C., "Rejection of Limit Cycles Induced from Disturbance Observers in Motion Control," IEEE Trans. on Industrial Electronics, Vol. 53, No. 6, pp. 1770-1780, 2006.
19. Choi, S. H., Ko, J. S., Kim, I. D., Park, J. S. and Hong, S. C., "Precise Position Control Using a PMSM with a Disturbance Observer Containing a System Parameter Compensator," IEE Proc.-Control Theory Application, Vol. 152, No. 6, pp. 1573-1577, 2005.
20. Lee, K. B., "Disturbance Observer that uses Radial Basis Function Networks for the Low Speed Control of a Servo Motor," IEE Proc.-Control Theory Application, Vol. 152, No. 2,

pp. 118-124, 2005.

21. Danesh, M., Sheikholeslam, F. and Keshmiri, M., "An Adaptive Manipulator Controller Based on Force and Parameter Estimation," IEICE Trans. Fundamentals of Electronic Communications and Computer Sciences, Vol. E89-A, No. 10, pp. 2803-2811, 2006.
22. Huang, Y. Y., Horng, R. H., Shih, Y. T. and Lee, A. C., "Dual-Position-Controller Design for the Linear-Motor-Driven Motion System," Journal of System Design and Dynamics, Vol. 1, No. 2, pp. 270-282, 2007.
23. Katsura, S., Matsumoto, Y. and Ohnishi, K., "Modeling of Force Sensing and Validation of Disturbance Observer for Force Control," IEEE Trans. on Industrial Electronics, Vol. 54, No. 1, pp. 530-538, 2007.
24. Su, W. T. and Liaw, C. M., "Adaptive Positioning Control for a LPMSM Drive Based on Adapted Inverse Model and Robust Disturbance Observer," IEEE Trans. on Power Electronics, Vol. 21, No. 2, pp. 505-517, 2006.
25. Bertoluzzo, M., Buja, G. S. and Stampacchia, E., "Performance Analysis of a High-Bandwidth Torque Disturbance Compensator," IEEE/ASME Trans. on Mechatronics, Vol. 9, No. 4, pp. 653-660, 2004.
26. Han, S. I., "Disturbance Observer-Based Sliding Mode Control for the Precise Mechanical System with the Bristle Friction Model," IJPEM, Vol. 4, No. 5, pp. 5-14, 2003.
27. Kobayashi, S., Awaya, I., Kuromaru, H. and Oshitani, K., "Dynamic Model Based Auto-tuning Digital Servo Driver," IEEE Trans. on Industrial Electronics, Vol. 42, No. 5, pp. 462-466, 1995.
28. Danaher Motion Company, "Kollmorgen: Platinum Ddl and Servostar setup Guide," Danaher Motion Company, Document No. M-LN-016-0702, 2002.
29. Edward, P. C., "Digital Filtering: An Introduction," Houghton Mifflin Co., pp. 479-483, 1992.
30. Choi, H. T., Kim, B. K., Suh, I. H. and Chung, W. K., "Design of Robust High-speed Motion Controller for a Plant with Actuator Saturation," ASME J. of Dynamic Systems, Measurement and Control, Vol. 122, No. 3, pp. 535-541, 2000.

APPENDIX

In the paper, one adopts the reference velocity v_r and reference acceleration $\dot{v}_r$ in our identification processes, i.e., assumptions $v = v_r$ and $\dot{v} = \dot{v}_r$ were made. If $v \neq v_r$ and $\dot{v} \neq \dot{v}_r$, the following equations are defined:

$$\begin{cases} v = v_r + \Delta v_r \\ \dot{v} = \dot{v}_r + \Delta \dot{v}_r \end{cases} \tag{A-1}$$

where Δv_r and $\Delta \dot{v}_r$ are velocity and acceleration following error, respectively. Moreover, multiplying Eq. (8) by $\dot{v}_r$ and integrating over a chosen period T_P, yield Eq. (A-2).

$$\begin{aligned} &\int_{T_p}(\hat{\tau}\dot{v}_r)dt = \int_{T_p}\Delta J(v\dot{v}_r)dt + \int_{T_p}\Delta B(v\dot{v}_r)dt + \int_{T_p}F_C\dot{v}_r dt + \int_{T_p}\delta\dot{v}_r dt \\ \Rightarrow &\int_{T_p}(\hat{\tau}\dot{v}_r)dt = \int_{T_p}\Delta J(\dot{v}_r + \Delta\dot{v}_r)\dot{v}_r dt + \int_{T_p}\Delta B(v_r + \Delta v_r)\dot{v}_r dt \\ &\quad + \int_{T_p}F_C\dot{v}_r dt + \int_{T_p}\delta\dot{v}_r dt \end{aligned} \tag{A-2}$$

and $\int_{T_p}F_C\dot{v}_r dt = 0$, $\int_{T_p}\delta\dot{v}_r dt \approx 0$. Eq. (A-2) can be simplified as

$$\int_{T_p}\hat{\tau}\dot{v}_r dt = \Delta J\int_{T_p}\dot{v}_r^2 dt + \Delta J\int_{T_p}(\Delta\dot{v}_r\dot{v}_r)dt + \Delta B\int_{T_p}(v_r\dot{v}_r)dt + \Delta B\int_{T_p}(\Delta v_r\dot{v}_r)dt \tag{A-3}$$

Given that $\Delta B\int_{T_p}(v_r\dot{v}_r)dt = 0$ and divide both sides of the above equation by $\int_{T_p}\dot{v}_r^2 dt$, one obtained,

$$\begin{aligned} \Delta J_r &= \frac{\int_{T_p}\hat{\tau}\dot{v}_r dt}{\int_{T_p}\dot{v}_r^2 dt} \\ &= \Delta J + \Delta J\frac{\int_{T_p}(\Delta\dot{v}_r\dot{v}_r)dt}{\int_{T_p}\dot{v}_r^2 dt} + \Delta B\frac{\int_{T_p}(\Delta v_r\dot{v}_r)dt}{\int_{T_p}\dot{v}_r^2 dt} \\ &= \Delta J + \Delta J\cdot\Theta_1 + \Delta B\cdot\Theta_2 \end{aligned} \tag{A-4}$$

where ΔJ_r denotes the inertia estimate error when considering the following errors. Compared with Eq. (16), the residual terms $\Delta J\cdot\Theta_1 + \Delta B\cdot\Theta_2$ caused by the following errors are found. In the same way, the following equation can also be obtained.

$$\begin{aligned} \Delta B_r &= \frac{\int_{T_p}\hat{\tau}v_r dt - F_C\int_{T_p}\hat{\tau}v_r dt}{\int_{T_p}v_r^2 dt} \\ &= \Delta B + \Delta J\frac{\int_{T_p}(\Delta\dot{v}_r v_r)dt}{\int_{T_p}v_r^2 dt} + \Delta B\frac{\int_{T_p}(\Delta v_r v_r)dt}{\int_{T_p}v_r^2 dt} \\ &= \Delta B + \Delta J\cdot\Theta_3 + \Delta B\cdot\Theta_4 \end{aligned} \tag{A-5}$$

where ΔB_r denotes the estimate error of viscous coefficient when considering the following errors.

Suppose the Coulomb friction F_C is known in advance. For the 1st iterative estimation process ($\Delta J^{(1)} = J - J_n^{(1)}$ and $\Delta B^{(1)} = B - B_n^{(1)}$), one obtains

$$\begin{aligned}\Delta J_r^{(1)} &= \frac{\int_{T_p}\hat{\tau}\dot{v}_r dt}{\int_{T_p}\dot{v}_r^2 dt} \\ &= \Delta J^{(1)} + \Delta J^{(1)}\frac{\int_{T_p}(\Delta\dot{v}_r\dot{v}_r)dt}{\int_{T_p}\dot{v}_r^2 dt} + \Delta B^{(1)}\frac{\int_{T_p}(\Delta v_r\dot{v}_r)dt}{\int_{T_p}\dot{v}_r^2 dt} \\ &= \Delta J^{(1)} + \Delta J^{(1)}\cdot\Theta_1 + \Delta B^{(1)}\cdot\Theta_2\end{aligned} \tag{A-6}$$

And

$$\begin{aligned}\Delta B_r^{(1)} &= \frac{\int_{T_p}\hat{\tau}v_r dt - F_C\int_{T_p}\hat{\tau}v_r dt}{\int_{T_p}v_r^2 dt} \\ &= \Delta B^{(1)} + \Delta J^{(1)}\frac{\int_{T_p}(\Delta\dot{v}_r v_r)dt}{\int_{T_p}v_r^2 dt} + \Delta B^{(1)}\frac{\int_{T_p}(\Delta v_r v_r)dt}{\int_{T_p}v_r^2 dt} \\ &= \Delta B^{(1)} + \Delta J^{(1)}\cdot\Theta_3 + \Delta B^{(1)}\cdot\Theta_4\end{aligned} \tag{A-7}$$

where the superscript $^{(n)}$ denotes the number of iteration. Update the inertia estimate,

$$\begin{aligned}\hat{J}_{new}^{(1)} &= \hat{J}_{old}^{(1)} + \Delta J_r^{(1)} \\ &= J_n^{(1)} + (\Delta J^{(1)} + \Delta J^{(1)}\cdot\Theta_1 + \Delta B^{(1)}\cdot\Theta_2) \\ &= J + (\Delta J^{(1)}\cdot\Theta_1 + \Delta B^{(1)}\cdot\Theta_2)\end{aligned} \tag{A-8}$$

Also, update the estimate of viscous coefficient,

$$\begin{aligned}\hat{B}_{new}^{(1)} &= \hat{B}_{old}^{(1)} + \Delta B_r^{(1)} \\ &= B_n^{(1)} + (\Delta B^{(1)} + \Delta J^{(1)}\cdot\Theta_3 + \Delta B^{(1)}\cdot\Theta_4) \\ &= B + (\Delta J^{(1)}\cdot\Theta_3 + \Delta B^{(1)}\cdot\Theta_4)\end{aligned} \tag{A-9}$$

For the 2nd iterative estimation process, one obtains

$$\begin{aligned}&\begin{cases}J_n^{(2)} = \hat{J}_{new}^{(1)} \\ B_n^{(2)} = \hat{B}_{new}^{(1)}\end{cases} \Leftrightarrow \begin{cases}\Delta J^{(2)} = J - J_n^{(2)} \\ \Delta B^{(2)} = B - B_n^{(2)}\end{cases} \\ &\Leftrightarrow \begin{cases}\Delta J^{(2)} = -\Delta J^{(1)}\cdot\Theta_1 - \Delta B^{(1)}\cdot\Theta_2 \\ \Delta B^{(2)} = -\Delta J^{(1)}\cdot\Theta_3 - \Delta B^{(1)}\cdot\Theta_4\end{cases}\end{aligned} \tag{A-10}$$

Substituting $\Delta J^{(2)}$ and $\Delta B^{(2)}$ into Eqs. (A-4) and (A-5) yields (A-11) and (A-12).

$$\begin{aligned}\Delta J_r^{(2)} &= \frac{\int_{T_p}\hat{\tau}\dot{v}_r dt}{\int_{T_p}\dot{v}_r^2 dt} \\ &= \Delta J^{(2)} + \Delta J^{(2)}\cdot\Theta_1 + \Delta B^{(2)}\cdot\Theta_2 \\ &= -(\Delta J^{(1)}\cdot\Theta_1 + \Delta B^{(1)}\cdot\Theta_2) - (\Delta J^{(1)}\cdot\Theta_1^2 + \Delta B^{(1)}\cdot\Theta_2\cdot\Theta_1) \\ &\quad - (\Delta J^{(1)}\cdot\Theta_3\cdot\Theta_2 + \Delta B^{(1)}\cdot\Theta_4\cdot\Theta_2)\end{aligned} \tag{A-11}$$

$$\begin{aligned}\Delta B_r^{(2)} &= \frac{\int_{T_p}\hat{\tau}v_r dt - F_C\int_{T_p}\hat{\tau}v_r dt}{\int_{T_p}v_r^2 dt} \\ &= \Delta B^{(2)} + \Delta J^{(2)}\cdot\Theta_3 + \Delta B^{(2)}\cdot\Theta_4 \\ &= -(\Delta J^{(1)}\cdot\Theta_3 + \Delta B^{(1)}\cdot\Theta_4) - (\Delta J^{(1)}\cdot\Theta_1\cdot\Theta_3 + \Delta B^{(1)}\cdot\Theta_2\cdot\Theta_3) \\ &\quad - (\Delta J^{(1)}\cdot\Theta_3\cdot\Theta_4 + \Delta B^{(1)}\cdot\Theta_4^2)\end{aligned} \tag{A-12}$$

Again, update the inertia estimate,

$$\begin{aligned}\hat{J}_{new}^{(2)} &= \hat{J}_{old}^{(2)} + \Delta J_r^{(2)} \\ &= (J + \Delta J^{(1)}\cdot\Theta_1 + \Delta B^{(1)}\cdot\Theta_2) - [(\Delta J^{(1)}\cdot\Theta_1 + \Delta B^{(1)}\cdot\Theta_2) \\ &\quad + (\Delta J^{(1)}\cdot\Theta_1^2 + \Delta B^{(1)}\cdot\Theta_2\cdot\Theta_1) \\ &\quad + (\Delta J^{(1)}\cdot\Theta_3\cdot\Theta_2 + \Delta B^{(1)}\cdot\Theta_4\cdot\Theta_2)] \\ &= J - (\Delta J^{(1)}\cdot\Theta_1^2 + \Delta B^{(1)}\cdot\Theta_2\cdot\Theta_1) \\ &\quad - (\Delta J^{(1)}\cdot\Theta_3\cdot\Theta_2 + \Delta B^{(1)}\cdot\Theta_4\cdot\Theta_2)\end{aligned} \tag{A-13}$$

Also, update the estimate of viscous coefficient,

$$\begin{aligned}\hat{B}_{new}^{(2)} &= \hat{B}_{old}^{(2)} + \Delta B_r^{(2)} \\ &= (B + \Delta J^{(1)}\cdot\Theta_3 + \Delta B^{(1)}\cdot\Theta_4) - [(\Delta J^{(1)}\cdot\Theta_3 + \Delta B^{(1)}\cdot\Theta_4) \\ &\quad + (\Delta J^{(1)}\cdot\Theta_1\cdot\Theta_3 + \Delta B^{(1)}\cdot\Theta_2\cdot\Theta_3) \\ &\quad + (\Delta J^{(1)}\cdot\Theta_3\cdot\Theta_4 + \Delta B^{(1)}\cdot\Theta_4^2)] \\ &= B - (\Delta J^{(1)}\cdot\Theta_1\cdot\Theta_3 + \Delta B^{(1)}\cdot\Theta_2\cdot\Theta_3) \\ &\quad - (\Delta J^{(1)}\cdot\Theta_3\cdot\Theta_4 + \Delta B^{(1)}\cdot\Theta_4^2)\end{aligned} \tag{A-14}$$

Similarly, for the 3rd iterative estimation process, one obtains

$$\begin{aligned}&\begin{cases}J_n^{(3)} = \hat{J}_{new}^{(2)} \\ B_n^{(3)} = \hat{B}_{new}^{(2)}\end{cases} \Leftrightarrow \begin{cases}\Delta J^{(3)} = J - J_n^{(3)} \\ \Delta B^{(3)} = B - B_n^{(3)}\end{cases} \\ &\Leftrightarrow \begin{cases}\Delta J^{(3)} = (\Delta J^{(1)}\Theta_1^2 + \Delta B^{(1)}\Theta_2\Theta_1) + (\Delta J^{(1)}\Theta_3\Theta_2 + \Delta B^{(1)}\Theta_4\Theta_2) \\ \Delta B^{(3)} = (\Delta J^{(1)}\Theta_1\Theta_3 + \Delta B^{(1)}\Theta_2\Theta_3) + (\Delta J^{(1)}\Theta_3\Theta_4 + \Delta B^{(1)}\Theta_4^2)\end{cases}\end{aligned} \tag{A-15}$$

Finally, the closed-form expression is obtained as follows.

$$\begin{bmatrix}\Delta J^{(n)} \\ \Delta B^{(n)}\end{bmatrix} = (-1)^{(n-1)}\cdot\begin{bmatrix}\Theta_1 & \Theta_2 \\ \Theta_3 & \Theta_4\end{bmatrix}^{(n-1)}\cdot\begin{bmatrix}\Delta J^{(1)} \\ \Delta B^{(1)}\end{bmatrix} \tag{A-16}$$

Convergence conditions

In the following, one will discuss the conditions for convergence when the proposed method suffers velocity and acceleration following errors. According to Eq. (A-16), the iterative estimation process will converge, if $\begin{bmatrix}\Theta_1 & \Theta_2 \\ \Theta_3 & \Theta_4\end{bmatrix}$ is a convergent matrix. The matrix can be decomposed as follows.

$$\begin{bmatrix}\Theta_1 & \Theta_2 \\ \Theta_3 & \Theta_4\end{bmatrix} = E_V\cdot\Sigma\cdot E_V^{-1} \tag{A-17}$$

where $\Sigma = \begin{bmatrix} \lambda_1 & \\ & \lambda_2 \end{bmatrix}$ is a diagonal matrix which is composed of eigenvalues of $\begin{bmatrix} \Theta_1 & \Theta_2 \\ \Theta_3 & \Theta_4 \end{bmatrix}$ and E_V is the corresponding eigenvector and

$$\begin{cases} \lambda_1 = \dfrac{\Theta_1 - \sqrt{4\Theta_2\Theta_3 + (\Theta_1 - \Theta_4)^2} + \Theta_4}{2} \\ \lambda_2 = \dfrac{\Theta_1 + \sqrt{4\Theta_2\Theta_3 + (\Theta_1 - \Theta_4)^2} + \Theta_4}{2} \end{cases} \tag{A-18}$$

$$E_V = \begin{bmatrix} -\dfrac{\Theta_1 + \sqrt{4\Theta_2\Theta_3 + (\Theta_1 - \Theta_4)^2} + \Theta_4}{2\Theta_3} & 1 \\ \dfrac{\Theta_1 + \sqrt{4\Theta_2\Theta_3 + (\Theta_1 - \Theta_4)^2} - \Theta_4}{2\Theta_3} & 1 \end{bmatrix}^T \tag{A-19}$$

Moreover

$$\begin{aligned} \begin{bmatrix} \Theta_1 & \Theta_2 \\ \Theta_3 & \Theta_4 \end{bmatrix}^{(n-1)} &= E_V \cdot \Sigma^{(n-1)} \cdot E_V^{-1} \\ &= E_V \cdot \begin{bmatrix} \lambda_1^{n-1} & \\ & \lambda_2^{n-1} \end{bmatrix} \cdot E_V^{-1} \end{aligned} \tag{A-20}$$

Notably, the process will converge if the following condition is satisfied.

$$\left| \frac{\Theta_1 \pm \sqrt{4\Theta_2\Theta_3 + (\Theta_1 - \Theta_4)^2} + \Theta_4}{2} \right| < 1 \tag{A-21}$$

Suppose the velocity command and its corresponding acceleration are,

$$\begin{cases} v_r = v_0 + v_1 \sin(\omega t) \\ \dot{v}_r = \omega \cdot v_1 \cos(\omega t) \end{cases} \tag{A-22}$$

Also, the velocity and acceleration responses are,

$$\begin{cases} v = v_0 + b \cdot v_1 \sin(\omega t + \phi) \\ \dot{v} = b \cdot \omega \cdot v_1 \cos(\omega t + \phi) \end{cases} \tag{A-23}$$

where b is a constant and ϕ is the corresponding phase lag, which can be obtained from the Bode diagram of the closed-loop system at frequency ω. Since the PI controller is applied, the DC-gain can be tuned to one so that the constant term on velocity remains the same. Then, the velocity and acceleration following errors can be obtained as follows.

$$\Delta v_r = v - v_r = v_1(-\sin(\omega t) + b\sin(\omega t + \phi)) \tag{A-24}$$

$$\Delta \dot{v}_r = \dot{v} - \dot{v}_r = \omega \cdot v_1(-\cos(\omega t) + b\cos(\omega t + \phi)) \tag{A-25}$$

Plugging Eqs. (A-22), (A-24) and (A-25) into Eq. (A-4) and Eq. (A-5), one obtained $\Theta_1 \sim \Theta_4$ in Eq. (A-21) as follows.

$$\Theta_1 = \frac{\int_{T_p} (\Delta \dot{v}_r \dot{v}_r) dt}{\int_{T_p} \dot{v}_r^2 dt} = \frac{\pi v_1^2 \omega (b\cos(\phi) - 1)}{\pi v_1^2 \omega} = b\cos(\phi) - 1 \tag{A-26}$$

$$\Theta_2 = \frac{\int_{T_p} (\Delta v_r \dot{v}_r) dt}{\int_{T_p} \dot{v}_r^2 dt} = \frac{b\pi v_1^2 \sin(\phi)}{\pi v_1^2 \omega} = \frac{b\sin(\phi)}{\omega} \tag{A-27}$$

$$\Theta_3 = \frac{\int_{T_p} (\Delta \dot{v}_r v_r) dt}{\int_{T_p} v_r^2 dt} = \frac{-b\pi v_1^2 \sin(\phi)}{\dfrac{\pi(v_1^2 + 2v_0^2)}{\omega}} = -\frac{-bv_1^2 \omega \sin(\phi)}{v_1^2 + 2v_0^2} \tag{A-28}$$

$$\Theta_4 = \frac{\int_{T_p} (\Delta v_r v_r) dt}{\int_{T_p} v_r^2 dt} = \frac{\dfrac{\pi v_1^2 (b\cos(\phi) - 1)}{\omega}}{\dfrac{\pi(v_1^2 + 2v_0^2)}{\omega}} = \frac{v_1^2 (b\cos(\phi) - 1)}{v_1^2 + 2v_0^2} \tag{A-29}$$

Substituting Eqs. (A-26)~(A-29) into Eq. (A-21) yields:

$$\left| \frac{(v_0^2 + v_1^2)(b\cos(\phi) - 1) \pm \sqrt{v_0^4 (b\cos(\phi) - 1)^2 - b^2 v_1^2 (2v_0^2 + v_1^2)\sin^2(\phi)}}{2v_0^2 + v_1^2} \right| < 1 \tag{A-30}$$

Notably, if $b \approx 1$ and $\phi \approx 0$, i.e., small tracking errors, then $|\lambda_i| << 1\,(i = 1, 2)$ and ΔJ and ΔB will converge toward zeros quickly. Thus, J_n approaches to J and B_n to B. If the Coulomb friction F_C is unknown, according to Eqs. (26) and (31), F_C will not affect the convergence conditions, Eq. (A-21) but only the convergence rate of ΔB and ΔJ.